



HAL
open science

The Influence of Wind on the Spatial Distribution of Pelagic Sargassum Aggregations in the Tropical Atlantic

Marine Laval, Yamina Aimene, Jacques Descloitres, Luc Courtrai, Paulo Duarte-Neto, Adán Salazar-Garibay, Pascal Zongo, René Dorville, Cristèle Chevalier

► To cite this version:

Marine Laval, Yamina Aimene, Jacques Descloitres, Luc Courtrai, Paulo Duarte-Neto, et al.. The Influence of Wind on the Spatial Distribution of Pelagic Sargassum Aggregations in the Tropical Atlantic. *Water*, 2025, 17 (6), pp.776. <10.3390/w17060776>. <hal-05074874>

HAL Id: hal-05074874

<https://hal.science/hal-05074874v1>

Submitted on 21 May 2025

HAL is a multi-disciplinary open access archive for the deposit and dissemination of scientific research documents, whether they are published or not. The documents may come from teaching and research institutions in France or abroad, or from public or private research centers.

L'archive ouverte pluridisciplinaire HAL, est destinée au dépôt et à la diffusion de documents scientifiques de niveau recherche, publiés ou non, émanant des établissements d'enseignement et de recherche français ou étrangers, des laboratoires publics ou privés.



Distributed under a Creative Commons CC BY 4.0 - Attribution - International License

Article

The Influence of Wind on the Spatial Distribution of Pelagic *Sargassum* Aggregations in the Tropical Atlantic

Marine Laval ^{1,2,*}, Yamina Aimene ¹, Jacques Descloitres ³, Luc Courtrai ⁴, Paulo Duarte-Neto ⁵ , Adán Salazar-Garibay ⁶, Alex Costa da Silva ⁷ , Pascal Zongo ¹ , René Dorville ¹ and Cristèle Chevalier ^{2,*}

- ¹ Laboratoire des Matériaux et Molécules en Milieu Agressif (L3MA) UR 4_1, UFR Science Technologie Environnement, Université des Antilles, 97233 Schoelcher, France
- ² Mediterranean Institute of Oceanography (MIO), IRD, Aix Marseille Université, CNRS, Université de Toulon, 13288 Marseille, France
- ³ Laboratoire d'Océanologie et de Géosciences (LOG) UMR 8187, University of Lille, CNRS, University Littoral Côte d'Opale, IRD, 59000 Lille, France
- ⁴ Institut de Recherche en Informatique et Systèmes Aléatoires (IRISA), Université de Bretagne Sud, 56000 Vannes, France
- ⁵ Departamento de Estatística e Informática (DEINFO), Universidade Federal Rural de Pernambuco (UFRPE), Rua Dom Manuel de Medeiros, s/n, Recife 52171-900, Brazil; paulo.duartent@ufrpe.br
- ⁶ Mexican Space Agency (AEM), Ciudad de Mexico 01020, Mexico
- ⁷ Departamento de Oceanografia da Universidade Federal de Pernambuco—DOCEAN/UFPE, Recife 50740-540, Brazil; alex.csilva@ufpe.br
- * Correspondence: marine.laval@etu.univ-antilles.fr (M.L.); cristele.chevalier@mio.osupytheas.fr (C.C.)

Abstract: Since 2011, *Sargassum* seaweed has spread widely outside the Sargasso Sea, causing massive strandings on the coasts of the West Indies and Mexico, causing serious economic, ecological, and health problems. This Atlantic pelagic alga has the characteristic of moving in rafts. According to in situ observations, their size and shape can vary with the wind. To better understand the effect of wind on *Sargassum* coverage and aggregation size, we conducted a large temporal (2019–2022) and spatial scale study in the West Indies using OLCI/Sentinel-3 satellite imagery. During this period, a database of nearly 1 million Sentinel-3 aggregations, including their geometric and wind characteristics, was established. Analysis of the size distribution showed that wind has a dual effect on disaggregation and agglomeration depending on wind speed and aggregation size: (1) low winds favor agglomeration for the smallest aggregations and disaggregation for the largest aggregations; (2) high winds favor disaggregation for all aggregation sizes. In addition, topography also plays a role in size distribution: the Caribbean arc favors agglomeration over offshore zones, and coastal areas favor disaggregation over offshore zones.

Keywords: *Sargassum* coverage; *Sargassum* aggregations; size distribution; wind speed; OLCI/Sentinel-3



Academic Editor: Guangyi Wang

Received: 6 September 2024

Revised: 25 October 2024

Accepted: 27 October 2024

Published: 7 March 2025

Citation: Laval, M.; Aimene, Y.; Descloitres, J.; Courtrai, L.; Duarte-Neto, P.; Salazar-Garibay, A.; Costa da Silva, A.; Zongo, P.; Dorville, R.; Chevalier, C. The Influence of Wind on the Spatial Distribution of Pelagic *Sargassum* Aggregations in the Tropical Atlantic. *Water* **2025**, *17*, 776. <https://doi.org/10.3390/w17060776>

Copyright: © 2025 by the authors. Licensee MDPI, Basel, Switzerland. This article is an open access article distributed under the terms and conditions of the Creative Commons Attribution (CC BY) license (<https://creativecommons.org/licenses/by/4.0/>).

1. Introduction

The Atlantic *Sargassum* algae of the genus *Sargassum* C. Agardh (Phaeophyceae, Fucales) have mainly been observed in the Sargasso Sea [1], located in the subtropical Atlantic gyre. However, since 2011, these brown macroalgae have been proliferating in a new area in the North Tropical Atlantic called “The Great *Sargassum* Belt” [2]. This area extends from the Gulf of Mexico to the West African coast through the Caribbean Sea. The coastlines in this area experience massive strandings during periods of strong proliferation of *Sargassum* [3–7]. These strandings harm the economy [8,9] and the ecology [10–13]. Furthermore,

the toxic gases (hydrogen sulfide and ammonia) emitted when decomposing and the high concentrations of heavy metals accumulated are a threat to public health [14–18].

In the Sargasso Sea and “The Great *Sargassum* Belt”, *Sargassum* seaweed refers to three morphotypes: *Sargassum natans* I Parr, *S. natans* VIII Parra, and *S. fluitans* III Parr [19–21]. These algae spend their entire lives drifting at the surface of the oceans and can form floating rafts. Rafts observed in the open sea are arranged in windrows and patches that range in size from tens of m² to several hundred km² [22–24]. The processes involved in the aggregation and dispersal of *Sargassum* rafts are not fully understood. However, in-situ observations of rafts [23,25–27] indicate that wind may play a role in raft shape and distribution, with aggregations being more elongated and aligned with the wind direction or dispersed in windy conditions [23,24,27,28]. Elongated rafts in windy conditions can be associated with Langmuir cells, resulting from Langmuir circulation that occurs at the surface of the oceans under the influence of the winds [29]. In contrast, larger and circular rafts have been observed in calm ocean conditions [22].

Some studies have also investigated the effect of wind on *Sargassum* distribution using spectral imagery, which allows for the collection of more spatial and temporal data. From a single day’s observations, Marmorino et al. [28] used high-resolution (~3 m) airborne imagery to observe the disintegration of *Sargassum* drift lines caused by wind. On a larger temporal and spatial scale, Sosa-Gutierrez et al. [30] and Sun et al. [31], using the Moderate Resolution Imaging Spectroradiometer (MODIS) sensor or the combination of multi-sensor output with MODIS, the Visible Infrared Imaging Radiometer Suite (VIIRS), and the Ocean Land Color Instrument (OLCI), observed a decrease in *Sargassum* coverage in the tropical Atlantic during extreme wind events associated with tropical cyclones conditions. However, they focus on extreme wind events only, while lower wind regimes have been poorly investigated.

This study aims to investigate and generalize the effect of wind, in non-extreme conditions, on *Sargassum* coverage and the *Sargassum* aggregation distribution. We analyze the distribution and dynamics of *Sargassum* rafts, especially on their disaggregation and agglomeration, over a range of low to moderate wind speeds (2 to 12 m·s⁻¹) using OLCI. The spatial resolution of the OLCI (300 m) allowed us to observe *Sargassum* aggregations (i.e., sets of rafts), while a MODIS resolution of 1 km did not. Furthermore, the short revisit time of 1 to 2 days provides good spatial coverage and temporal sampling. In the current analysis, four years of *Sargassum* and wind data in the West Indies at the Lesser Antilles Arc location, an area heavily affected by *Sargassum* inundation, were gathered and analyzed.

2. Materials and Methods

2.1. Study Area

The selected study area is centered around the Lesser Antilles Arc, located at 8° to 22° latitude and -75° to -47° longitude (Figure 1). The Lesser Antilles Arc borders the Caribbean Sea to the west and the Atlantic Ocean to the east. This area is part of the “Great *Sargassum* Belt” and has been subject to a large and increasing influx of *Sargassum* since 2011 [32,33], except for a few years [34]. The abundance of *Sargassum* varies seasonally, with the highest concentrations occurring from April to August and the lowest concentrations from September to January [33–35]. During periods of high *Sargassum* concentrations, large strandings occur on the Caribbean coasts and the islands of the West Indies, especially on the islands of the Lesser Antilles Arc [6,7,33,36].

To better assess the effect of wind on the *Sargassum* strandings and distribution, the study area was divided into 5 zones. This division is motivated by differences in oceanic dynamics and the abundance of *Sargassum* in these zones (Figure 1):

- The coastal zone (Coastal) extends within 30 km from the coasts;

- The Atlantic Antilles Zone (AAZ) (Atlantic close-offshore area) is delimited by an outer arc 150 km east of the Antilles arc (encompassing but not including the coastal zone);
- The Atlantic Zone (AZ) (Atlantic far-offshore area) extends beyond the AAZ to the Atlantic Ocean;
- The Caribbean Antilles Zone (CAZ) (Caribbean close-offshore area) is delimited by an outer arc 150 km west of the Antilles arc (encompassing but not including the coastal zone);
- The Caribbean Zone (CZ) (Caribbean far-offshore area) extends beyond the CAZ to the Caribbean Sea.

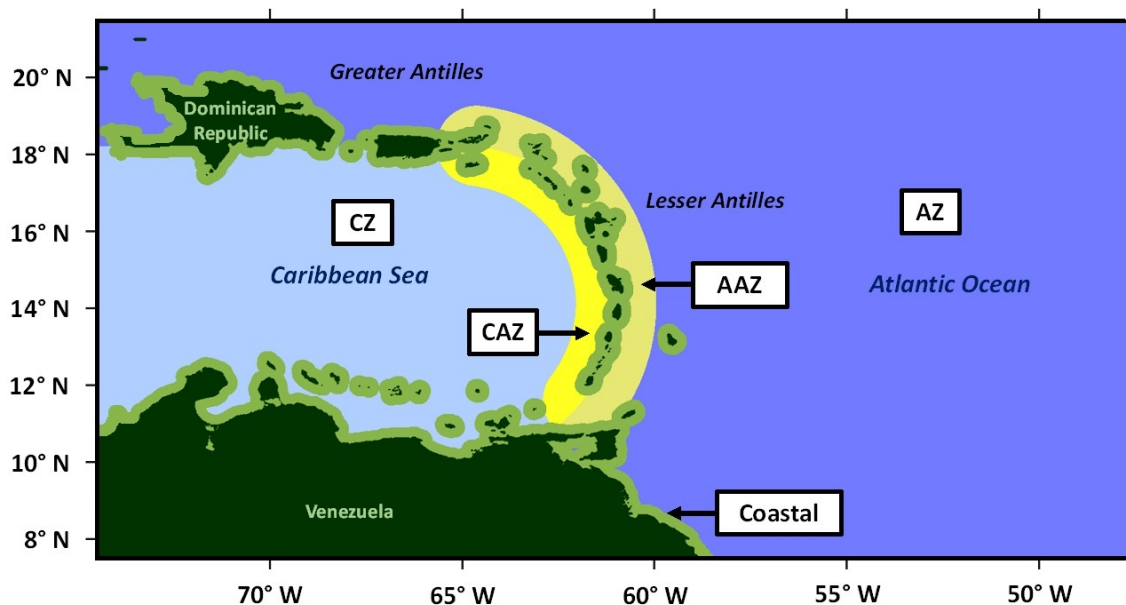


Figure 1. Zones of the study area: Caribbean Zone (CZ), Atlantic Zone (AZ), Caribbean Antilles Zone (CAZ), Atlantic Antilles Zone (AAZ), and the coastal zone. Land areas are shown in dark green.

The *Sargassum* found in the Caribbean Sea is mainly brought by the Atlantic currents passing through the Lesser Antilles Arc, including the North Equatorial Guinea eddies and the reverse front of the North Brazil Current [33,35–38]. The different zones allow the study of the spatial effects on the distribution of *Sargassum*.

2.2. *Sargassum* Dataset

The *Sargassum* data used in this study are derived from the OLCI satellite sensor. OLCI is an instrument on board the Sentinel-3A and Sentinel-3B satellites launched in 2016 and 2018, respectively, by the European Union’s Copernicus Earth Observation Programme. The satellite images obtained by both OLCI sensors have a spatial resolution of 300 m/pixel with a swath width of 1270 km. Each of the two Sentinel-3 satellites has a revisit period of 1 to 2 days. The combination of the two satellites provided almost complete coverage of the study area every day. Our study period covers 1249 days from 2019 to 2022. Each OLCI satellite image was processed using a deep learning model to detect pixels containing *Sargassum*, as described by Laval et al. [39]. The images obtained using this method contain binary information about whether a pixel contains *Sargassum*.

2.3. Atmospheric Data

2.3.1. Wind

The surface wind data used are from the ERA5 reanalysis dataset [40], namely the zonal and meridional components of the wind, u and v , at 10 m every hour with a spatial

resolution of $1/4^\circ$ (available at <https://cds.climate.copernicus.eu/>, accessed on 28 October 2024). The temporal variability of the wind speed is analyzed using a moving mean over the study area (Figure 1) and the study period from 2019 to 2022. The wind model grid was interpolated to the resolution of the OLCI images to be associated with the satellite image pixels.

2.3.2. Cloud Fraction

A cloud mask was created for each day from the same OLCI images used for *Sargassum*. The cloud mask was calculated using the 754 nm and 865 nm bands of OLCI from the method adapted from [41] for MODIS by Schamberger et al. [42]. The cloud fraction was calculated as the ratio of cloud pixels to the total number of pixels in each area, excluding land pixels, for each day over the entire period.

2.4. *Sargassum* and Water Fraction

The fraction of water in a given area is defined as the number of cloud-free water pixels out of the total number of pixels:

$$\text{Water fraction} = \frac{\text{Number of water pixels}}{\text{Number total of pixels}} \quad (1)$$

Water pixels include *Sargassum* and *Sargassum*-free pixels. The total number of pixels includes water and cloud pixels without land pixels.

The fraction of *Sargassum* pixels (or *Sargassum* fraction in short) in a given area is the number of pixels containing *Sargassum* over the total number of cloud-free water pixels:

$$\text{Sargassum fraction} = \frac{\text{Number of Sargassum pixels}}{\text{Number of water pixels}} \quad (2)$$

The fractions vary between 0 and 1. The temporal variability of the *Sargassum* fraction is analyzed using a moving mean over 30 days (Figure 2).

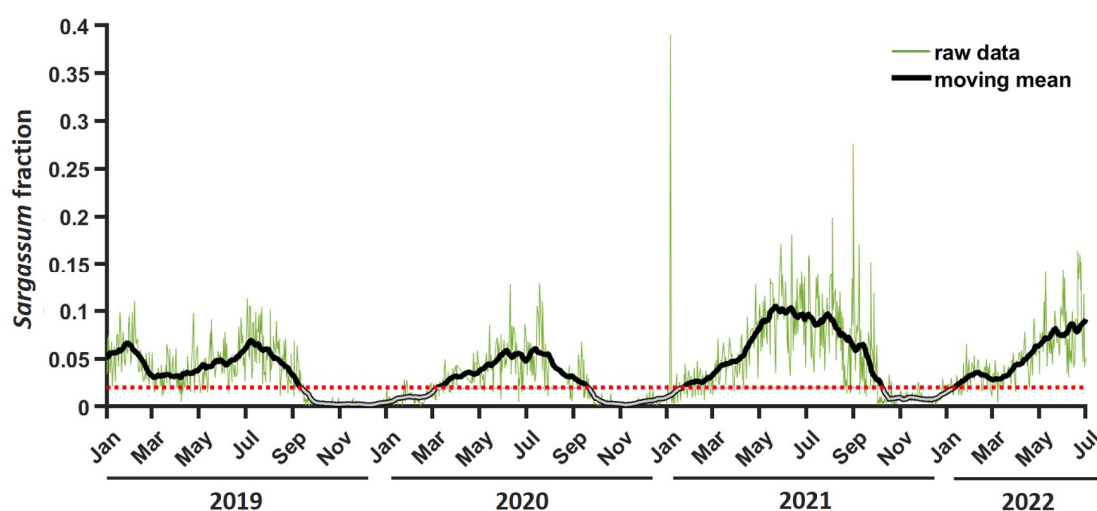


Figure 2. Temporal variation in the *Sargassum* fraction (green line) and its moving mean (black line) in the whole study area between 2019 and 2022. Periods of low *Sargassum* fraction with a moving mean below 0.02 (dashed red horizontal line) are shown in gray.

2.5. *Sargassum* Aggregation Parameters

A *Sargassum* aggregation is an indivisible group of *Sargassum* rafts in satellite imagery [39]. Here, we define an aggregation as a set of pixels that share a common side

or vertex between pixels or an isolated pixel (Figure 3). Around one million *Sargassum* aggregations were tagged between 2019 and 2022.

For each aggregation, geometric parameters were defined: area, length, width, and location of the aggregation. The area of an aggregation is defined as the number of pixels in the aggregation. The other geometric parameters are determined using a reference ellipse that represents the shape of the aggregation (Figure 3). The center of the reference ellipse is the centroid of the aggregation. The minor and major axes of the reference ellipse are such that the ellipse has the same second moment of area as the aggregation (hence not the same area). The aggregation geometric parameters are then defined as follows:

- The length corresponds to the major axis of the reference ellipse;
- The width corresponds to the minor axis of the reference ellipse, perpendicular to the major axis;
- The location is defined by the center of the reference ellipse by longitude and latitude. The location is used to assign *Sargassum* aggregations to zones and wind components.

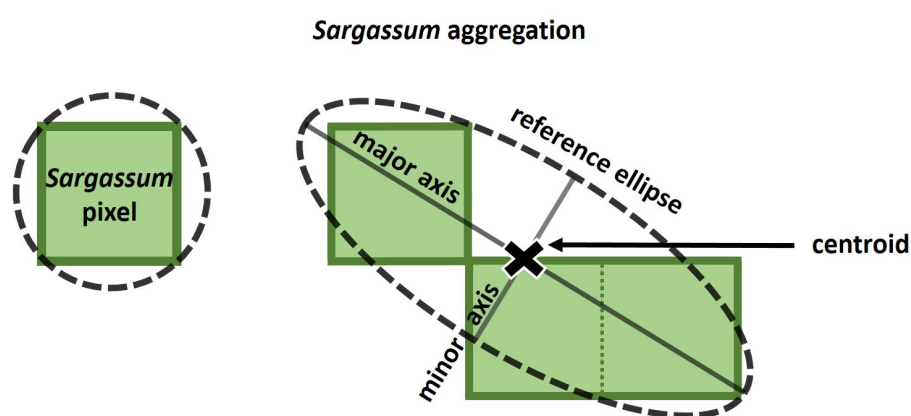


Figure 3. Diagram of a *Sargassum* aggregation and the characteristics derived from its reference ellipse: major axis, minor axis, and center.

The smallest reference ellipse, corresponding to a single-pixel aggregation, has a length and width of 1.15 pixels (i.e., a circle of 0.35 km diameter) with the same second moment of area of $1.35 \times 10^{-3} \text{ km}^4$ for both.

2.6. Representation of the Size of *Sargassum* Aggregations

We chose the area as a proxy for the size of the aggregations, while the length and width were used only to characterize the shape. As mentioned in Section 2.5, about 1 million aggregations were analyzed, with areas ranging from 1 pixel to many pixels. In the following, the aggregation surface area is studied as a continuous variable described by classes, $[A_i, A_{i+1}[$, whose limits are the successive terms of the geometric sequence with first member A_0 and ratio 2. Then, the general term is

$$A_i = A_0 2^i; i = 1, \dots, n \tag{3}$$

with n as the class range corresponding to the largest area found in the whole dataset. The possible smallest surface area, A_0 , is 1 pixel, i.e., $A_0 = 0.3 \text{ km} \times 0.3 \text{ km} = 0.09 \text{ km}^2$.

The mode value was not estimated from the modal class but rather from the distribution’s probability density function to characterize the surface area distribution. This approach was chosen because it provides a more accurate representation of the mode, especially in skewed distributions where the modal class might not capture the peak accurately. The variation in the distribution at the left and right of the mode was characterized by two

linear regressions on a logarithmic scale. Here, the logarithm used in these regressions is the decimal logarithm.

$$\log_{10}(p) = k \log_{10}(A) + \log_{10}(a) \tag{4}$$

with p as the probability density, k as the slope in the logarithmic axis, and $\log_{10}(a)$ as the intercept (the intersection value with the y-axis). Alternately, p can be expressed as a power law, $p = a A^k$. Although $\log_{10}(a)$ and a appear in the equations, it is not explicitly used for interpretation in this article; we focus solely on the slope value.

2.7. Dataset Selection

2.7.1. Image Selection Using *Sargassum* Fraction

For the analysis, we only included periods when *Sargassum* is consistently present in the study area to avoid seasonal bias. Periods with consistent *Sargassum* presence are defined as having the running mean of the *Sargassum* fraction being greater than 0.02. Figure 2 shows that the corresponding periods are from March to September, which includes the April to August period of the highest occurrence of *Sargassum* strandings in the study area according to local observations and as reported by [33], as well as January, February, and October, depending on the year. Furthermore, within the selected period, we discarded images with a *Sargassum* fraction lower than 0.01. Using these criteria, we retained about 68% of the initial images (i.e., 851 of 1249).

This selection, based on the *Sargassum* fraction, allowed us to limit the analysis to periods of effective presence of *Sargassum* in the study area, thus eliminating any wrong conclusions related to the wind effect on *Sargassum* presence.

2.7.2. Image Selection Using Cloud Fraction

Cloud fraction in the satellite images is another factor used to select our samples. Figure 4 shows the *Sargassum* fraction as a function of cloud cover. The median of the *Sargassum* fraction is constant, around 0.05, for a cloud fraction between 0 and 0.7. When the cloud fraction is greater than 0.7, the *Sargassum* fraction median decreases to reach half that value (0.025). This may indicate that the related images are not representative of calculating the *Sargassum* fraction, and this could introduce a bias. Because only a few images were concerned (7 images), they were removed. Therefore, our final sample is now composed of 844 images.

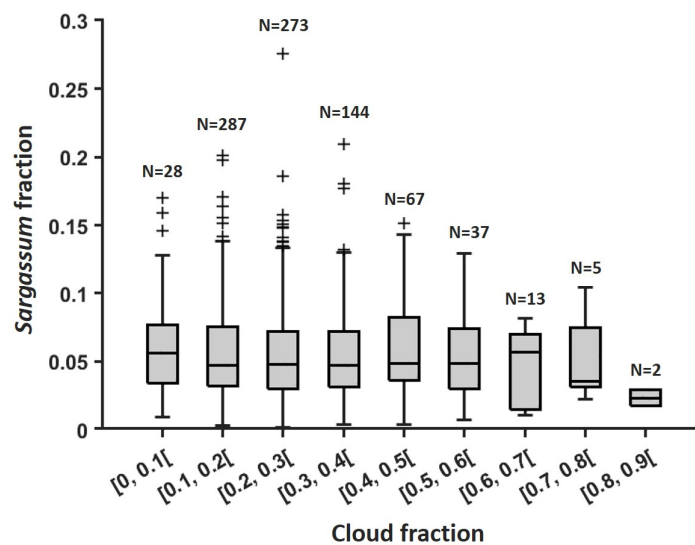


Figure 4. Boxplot of *Sargassum* fraction as a function of cloud fraction. “+” indicates the outlier data not considered in the boxplot estimation.

2.7.3. Selection of Wind Speed Range

To define the range of wind speed available for analysis in the satellite dataset, we computed the distribution of images against wind speed (Figure 5). We defined 16 wind classes between 0 and 16 m·s⁻¹, with a 1 m·s⁻¹ range each. For each image and each wind class present in the image, the water and *Sargassum* fractions (Equations (1) and (2)) were calculated. Low water fractions and low *Sargassum* fractions (less than 0.05 and 0.001, respectively) were discarded, as they were not considered representative for this study. Based on those criteria, Figure 5 (dark bars) shows that only very few images (15 or less) contribute to wind classes outside to [2, 12[m·s⁻¹. Therefore, we only analyzed the classes between 2 and 12 m·s⁻¹ in this study.

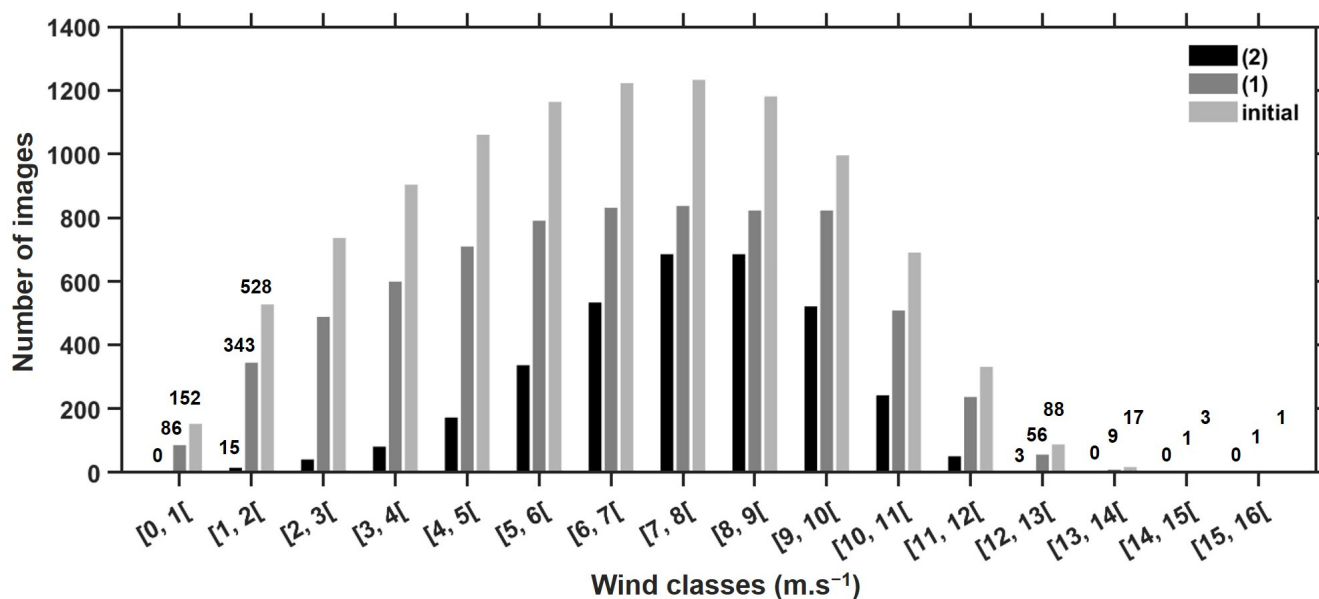


Figure 5. The number of images for each wind class, for the different sampling of the satellite images: (1) sample outside the *Sargassum* period, high cloud fraction, and low *Sargassum* abundance; (2) after deletion of classes unrepresentative of water and *Sargassum* fraction.

To illustrate the impact of sample selection using the *Sargassum* fraction, cloud fraction, and water fraction on the wind classes, Figure 5 shows the samples available for each wind class before and after reducing the dataset.

3. Results

3.1. Temporal Variation in Wind, Cloud Fraction, and *Sargassum* Fraction

3.1.1. Wind Variability

Over the entire timeframe of the study and the entire study area, the winds varied between 0.002 and 20 m·s⁻¹. The mean wind from the moving mean has similar variability between the Caribbean (CZ + CAZ) and Atlantic (AZ + AAZ) zones, as illustrated by Figure 6. We distinguish a period of high wind and a period of low wind, observed around the well-known dry and wet seasons of the region. The high wind season is slightly longer in the Caribbean zone (8 months, from January to August) than in the Atlantic zone (7 months, from January to July). Globally, winds are stronger in the Caribbean zone compared with the Atlantic zone (mean wind 8.5 m·s⁻¹ and 7.5 m·s⁻¹, respectively). Therefore, the weak wind season is shorter in the Caribbean zone (4 months, from September to December) than in the Atlantic zone (5 months, from August to December). Winds are weaker in the Atlantic zone, with a mean wind of 7.5 m·s⁻¹ and 6.5 m·s⁻¹ in the Caribbean

zone. The minimum wind is $5.5 \text{ m}\cdot\text{s}^{-1}$ in September in the Caribbean zone, whereas it can reach a minimum of $4.5 \text{ m}\cdot\text{s}^{-1}$ in the Atlantic zone.

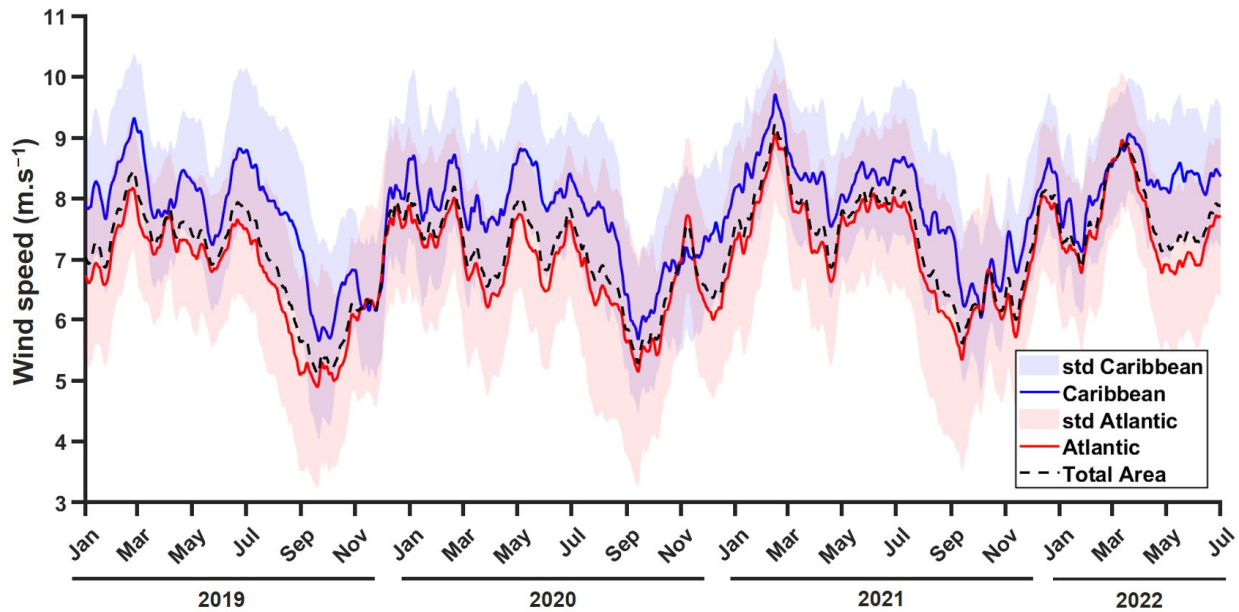


Figure 6. Moving mean of wind speed from 2019 to 2022, outside the coastal zone, for the whole study area (dashed black line), the Caribbean zone (CZ + CAZ; solid blue line) with its standard deviation (solid blue zone), and the Atlantic zone (AZ + AAZ, solid red line) with its standard deviation (solid red zone).

3.1.2. Cloud Fraction Variability

Over the four years of the study, the distribution of cloud fraction within the same month is highly variable (Figure 7). April to June and August to November showed the highest medians, above 0.2, and the largest standard deviations. For these months, maxima above 0.6 of the cloud fraction are observed. For December to March and July, the median is most often below 0.2 of the cloud fraction. The standard deviation variation is smaller than for other months.

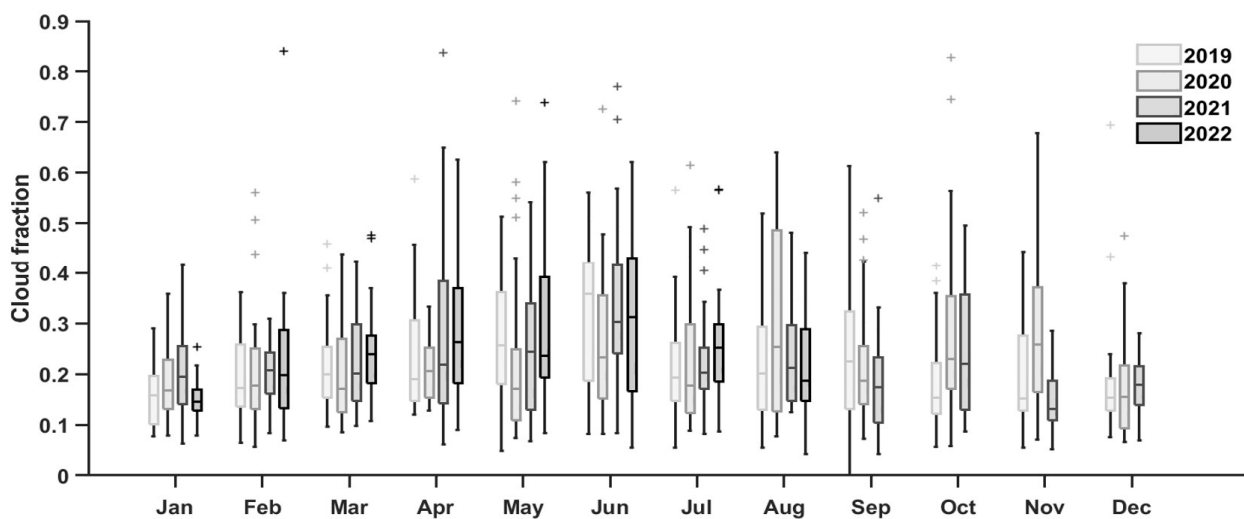


Figure 7. Monthly distribution of cloud fraction for 2019, 2020, 2021, and 2022, illustrated by boxplot. “+” indicates the outlier data not considered in the boxplot estimation.

3.1.3. *Sargassum* Fraction Variability

First, in the study area, the *Sargassum* fraction in the total area increased from January to May, peaked in the May–July period (average *Sargassum* fraction between 0.06 and 0.12), and decreased from July to October (Figure 8; black curve). Between October and January, the average *Sargassum* fraction is the lowest, below 0.02, as illustrated in Figure 2 as well. The period of low *Sargassum* fraction decreased as time went on, from 6 months in 2019 to 3 months in 2021. Over the four years, a second peak occurring earlier in February was observed, usually much smaller (average fraction between 0.01 and 0.04) compared with the May–July peak, except in 2019, where the amplitudes of both peaks are similar (0.06 of the average fraction).

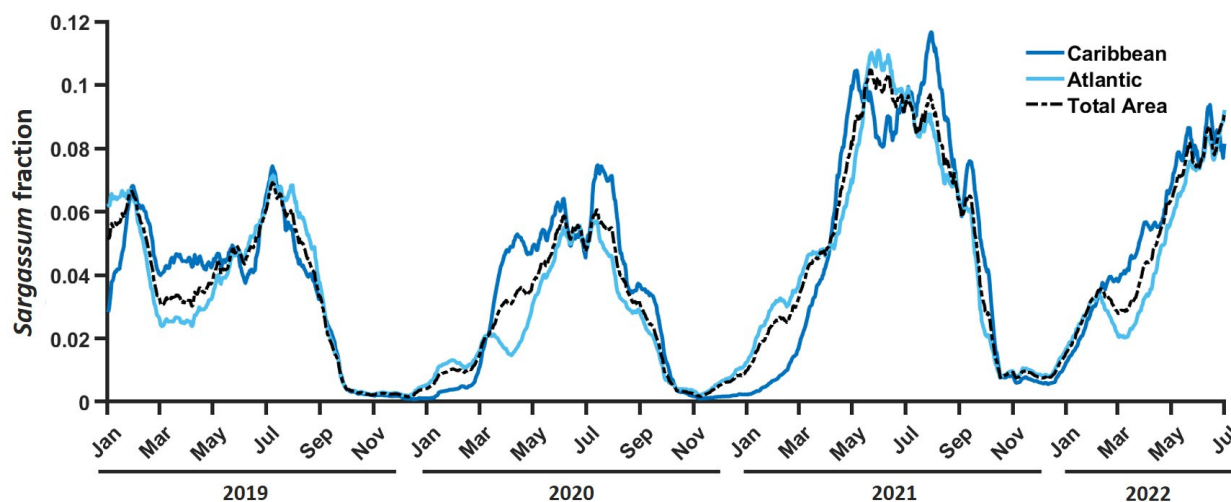


Figure 8. Moving mean of *Sargassum* fraction from 2019 to 2022 for the entire study area (dashed black line), the Caribbean zone (CZ + CAZ; solid dark blue line), and the Atlantic zone (AZ + AAZ, solid light blue line).

The variation in the *Sargassum* fraction exhibited the same trend in the Caribbean (CZ + CAZ) and Atlantic (AZ + AAZ) zones. However, there is a time lag of about 1 month in the arrival of the *Sargassum* between the two zones, with an increase in the *Sargassum* fraction first seen in the Atlantic zone, then in the Caribbean zone. The *Sargassum* fraction is the highest in the Atlantic zone from January to March and in the Caribbean zone from March to October. The *Sargassum* season is longer in the Caribbean zone than in the Atlantic zone, lasting, respectively, from April to September and May to August.

The seasonal variation in *Sargassum* coverage usually observed in this zone, with a peak around June [2,31,33,43,44], is also observed in our data, with a slight shift between the tropical Atlantic zone and the Caribbean Sea (Figure 8). This shift is related to the connectivity between the two zones, *Sargassum* is transported from the Atlantic to the Caribbean through the Lesser Antilles Arc from spring to early fall by the Guiana Current, the North Brazil Current Rings, and the North Brazil Retroflexion Current [33,35,37,43].

3.2. OLCI *Sargassum* Aggregations

3.2.1. Geometrical Characteristics of *Sargassum* Aggregations

In the area of interest from 2019 to 2022, during the *Sargassum* period, the *Sargassum* aggregation geometrical characteristics are distributed within a large range of values: areas ranging from 0.09 km² to 32,000 km², length from 0.35 km to 760 km, and width from 0.35 km to 290 km). Even though their distribution is extensive (Table 1), we observe the following:

- A total of 25% of the aggregation areas are smaller than 1.1 km², 50% are smaller than 4.7 km², 75% are smaller than 18 km², 90% are smaller than 53 km², and 99% are smaller than 500 km²;
- A total of 25% of the aggregation lengths are smaller than 1.5 km, 50% are smaller than 3.4 km, and 90% are smaller than 17 km;
- A total of 25% of the aggregation widths are smaller than 1.1 km, 50% are smaller than 1.7 km, and 90% are smaller than 4.9 km.

Table 1. Statistics on geometric characteristics of *Sargassum* aggregations (the ratio is not the ratio of medians of the length and width in the table but rather the median of the ratio W/L).

Characteristics/ Statistics	D1 (10%)	Q1 (25%)	Q2 (Median) (50%)	Q3 (75%)	D9 (90%)	Min–Max
Area (km ²)	0.27	1.1	4.7	18	53	0.09–32,577
Length (km) (Major axis length)	0.69	1.5	3.4	8.1	17	0.35–760
Width (km) (Minor axis length)	0.35	1.0	1.8	3.1	5.3	0.35–242

One can notice that 50% of the aggregations have an area between 1.1 km² and 18 km² and 80% between 0.27 km² and 53 km².

Sargassum raft shapes have been described to range from circular to very elongated, or even in the form of filaments [24]. The ratio W/L is considered in the following to address the shapes of our aggregations. As illustrated in Figure 9, it decreases (i.e., the aggregations become more elongated) as the surface area increases. As illustrated in Table 1:

- The smallest 10% of aggregations (i.e., for $A \leq 0.27 \text{ km}^2$) are mainly circular to slightly elongated: $0.50 \leq W/L \leq 1$;
- The aggregations in the range $0.27 \text{ km}^2 \leq A \leq 4.7 \text{ km}^2$ (i.e., 40%) are slightly elongated to elongated: $0.50 \leq W/L \leq 0.75$;
- The aggregations in the range $4.7 \text{ km}^2 \leq A \leq 18 \text{ km}^2$ (i.e., 25%) are elongated: $0.35 \leq W/L \leq 0.67$; 25%;
- The largest 25% of aggregations (i.e., $A \geq 18 \text{ km}^2$) are very elongated ($0.20 \leq W/L \leq 0.45$).

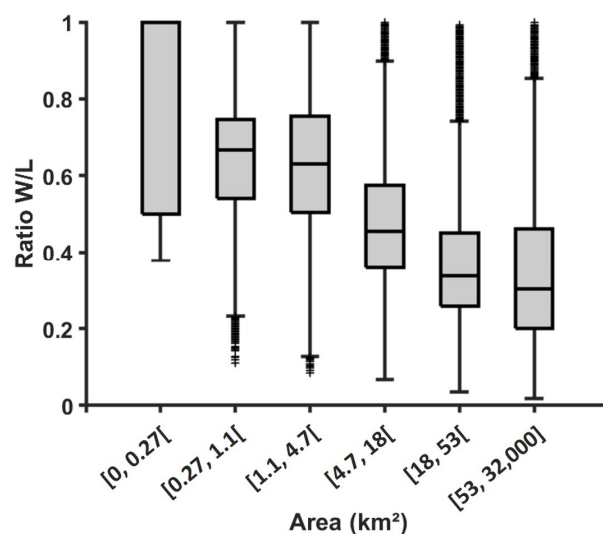


Figure 9. Boxplot of the ratio W/L distribution as a function of the area classes corresponding to the distribution quantiles and deciles.

Aggregation surface areas smaller than 0.27 km^2 (area of 3 pixels, about 10% of the sample), do have the most variable W/L ratio ($0.5 \leq W/L \leq 1$) (Figure 9). Three-pixel aggregations have a very limited spatial arrangement, ranging from circles to elongated ellipses. Single-pixel aggregations (6% of the sample) are circles, and two-pixel aggregations (3%) are elongated ellipses ($W/L = 0.4$ or $W/L = 0.5$).

It is important to keep in mind that the OLCI *Sargassum* aggregations are a set of *Sargassum* rafts (cf. Section 2.5). *Sargassum* rafts are smaller (typical area size is around ten square meters) [24,27] than the OLCI resolution ($300 \text{ m} \times 300 \text{ m}$). Aggregation length and width, determined from the reference ellipse, are also longer than the raft dimensions. Besides, they are related to the aggregation surface area; for a given area by the OLCI pixels, the aggregation length and width can be determined using a second-order polynomial function that was the best fit of length and width as a function of area (Figure A1).

3.2.2. Area Distribution of *Sargassum* Aggregations

The probability density function of area classes follows the appearance of an asymmetric distribution with negative skewness (Pearson's first skewness = -0.42), indicating that the mode is to the right of the mean. The modal class, i.e., the most represented area class of our dataset, is $[6.76, 11.5[\text{ km}^2$ (Figure 10), and the mode from the density probability function is 7.5 km^2 , which is higher than the median (4.7 km^2) and mean (4.3 km^2).

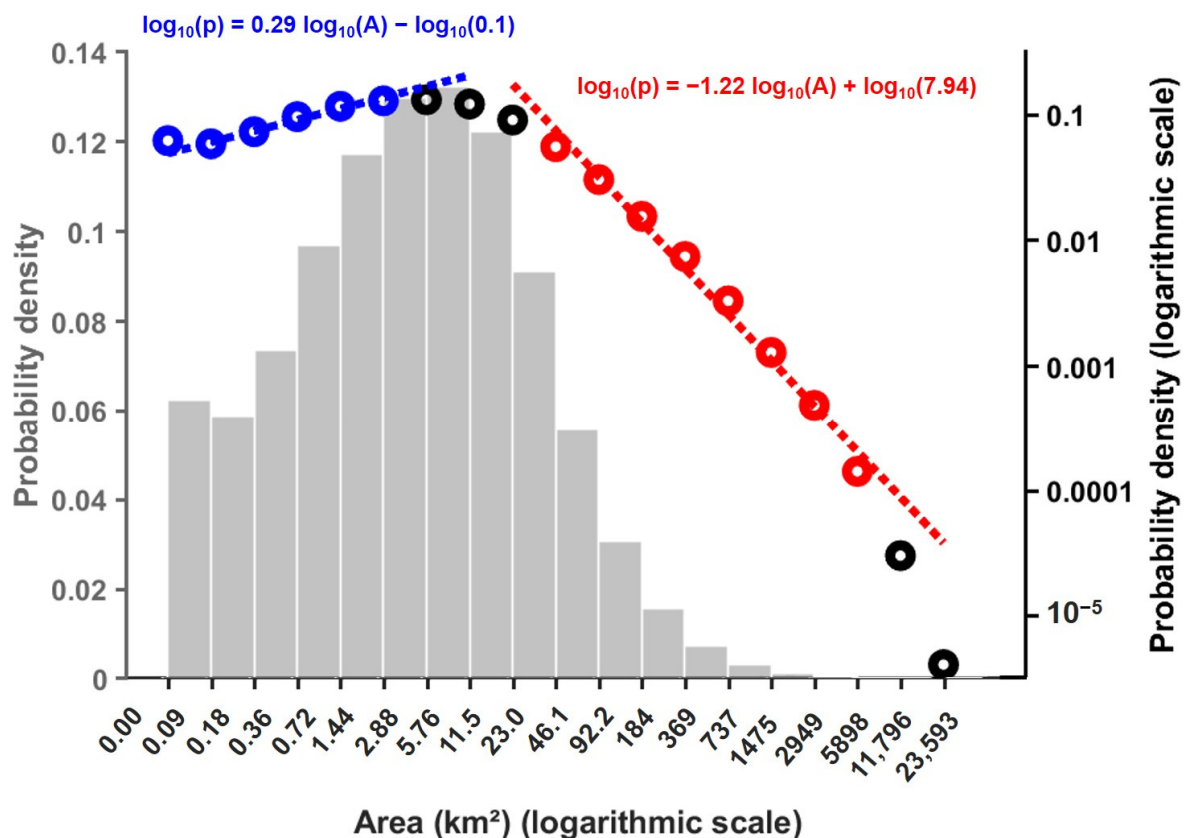


Figure 10. Distribution of the area of *Sargassum* aggregations represented by (i) the histogram of the area classes (gray bars) and its probability density function (gray line), indicated by the left y-axis, and (ii) dots representing the distribution of the area classes on a logarithmic scale indicated in the right y-axis. The red and blue points correspond to those used to estimate the linear regressions, represented by the dashed red and blue lines, respectively.

The modal class divides the surface area dataset into two subsets (Figure 10): a subset on the left side of the mode (left subset) with small OLCI aggregations (area classes

between 0 to 6 km²) and a subset on the right side of the mode (right subset) with large OLCI aggregations (area classes between 6 to 32,000 km²).

The first class, [0.09, 0.18[km², is a special class with more aggregations than the next (Figures 9 and 10). In conjunction with the OLCI resolution, *Sargassum* aggregations smaller than 1 pixel (0.09 km²) are all classified in this first class.

Except for this first class, in the left subset, the number of aggregations per area class increases with size. The slope of the left logarithmic distribution (left slope) is around 0.29. On the other hand, the number of aggregations of the right subset decreases with size, and the slope of the right logarithmic distribution (right slope) is around -1.22. This slope is steeper than the slope on the left side.

3.2.3. Spatial Variation in *Sargassum* Aggregation Area Distribution

The size distribution of aggregations varies spatially. This is illustrated by the mode and the two slopes, presented in Figure 11. The major observations are as follows:

- Three different mode values can be observed. The CAZ mode is the highest (6.82 km²); it is a little bit lower than the global mode. CZ and AAZ are around 5 km² (5.35 and 5.19 km²). The Coastal area and the AZ are the smallest, with a value of about 3.5 km² (3.65 and 3.56 km²).
- The left slope is almost constant around 0.3 (between 0.31 and 0.35), except in the CZ zone, where it reduces to 0.26.
- The highest negative right slope is observed in the coastal zone (-1.67), and the lowest is in the CAZ zone (-1.04), followed by the AAZ zone (-1.14). The CZ and AZ zones have medium and quite similar slopes (-1.28 and -1.26 resp.).

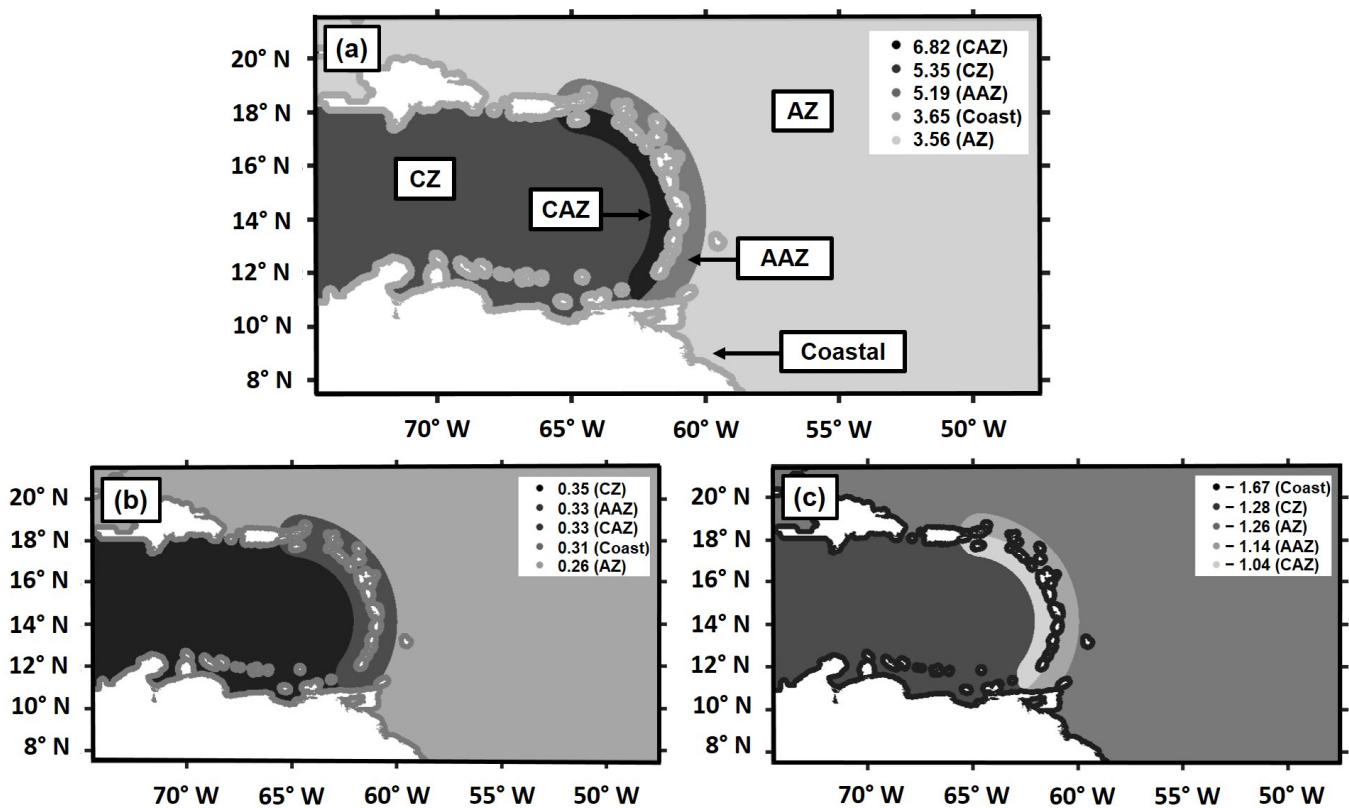


Figure 11. Values of (a) the mode, (b) the left slope, and (c) the right slope of the surface area distribution as a function of the zones (Coastal, CZ, AZ, AAZ, and CAZ).

3.3. Distribution of Sargassum Fraction and Aggregation Area as a Function of Wind Speed

3.3.1. Influence of Wind on Sargassum Fraction

The average *Sargassum* fraction decreases by 0.05 in each considered wind speed class (Figure 12). The same global tendency is observed for each month between January to September. The monthly averages for the *Sargassum* fraction from January to April and September are lower than the overall average for the *Sargassum* fraction, while they are higher for May to August. The maximum difference in the monthly *Sargassum* fraction is 0.06, observed between July and September. Consequently, the maximum estimated standard deviation is about 0.08, observed for weak wind speeds; the overall standard deviation envelope decreases and narrows as the wind increases.

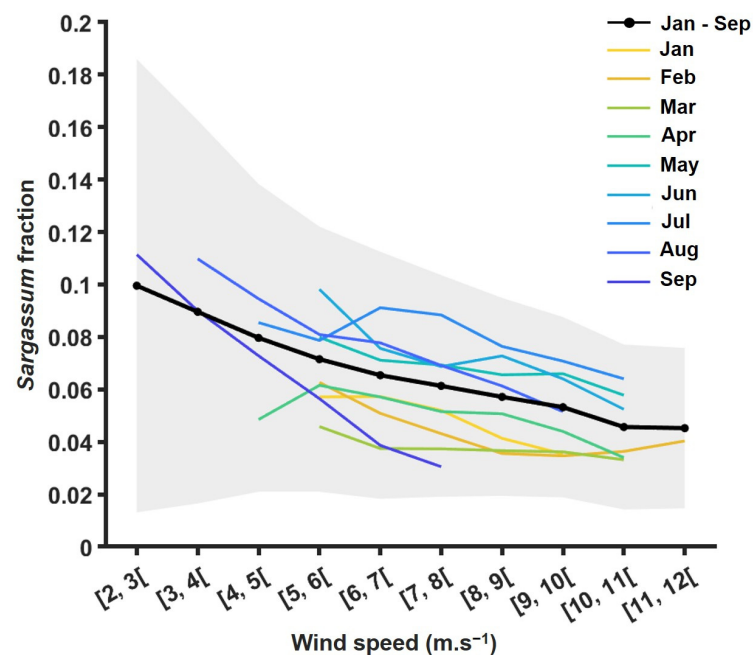


Figure 12. Average *Sargassum* fraction in each wind class (black line) and per month from January to September (yellow to blue lines). The gray envelope represents the standard deviation of the average *Sargassum* fraction.

3.3.2. Influence of Wind on the Distribution of *Sargassum* Aggregations

The variation in the mode, the left slope, and the right slope increases with the wind speed until the wind speed reaches $[8, 9[$; $[7, 8[$ and $[9, 10[$ $\text{m}\cdot\text{s}^{-1}$, respectively (Figure 13). At these wind classes, the respective parameters reach their extremum and then decrease. The mode increases from 3.6 km^2 to reach its maximum of 5 km^2 in the wind class $[8, 9[$ $\text{m}\cdot\text{s}^{-1}$ and decreases until reaching the value of 4.1 km^2 with a wind speed of $[11, 12[$ $\text{m}\cdot\text{s}^{-1}$. The right slope increases from 0.97 to reach its maximum of 1.3 in the wind class $[9, 10[$ $\text{m}\cdot\text{s}^{-1}$ and decreases until 1.02 for the maximum studied wind. On the other hand, the left slope is almost constant, with a slight increase from 0.26 to 0.31 reached in the $[7, 8[$ $\text{m}\cdot\text{s}^{-1}$ wind class, followed by a slightly stronger decrease to reach 0.23 at the maximum wind speed.

Please note, for the right slope of the $[9, 10[$ $\text{m}\cdot\text{s}^{-1}$ wind class and above, the number of area classes available for the calculation of the linear regression gradually decreases from nine to five classes.

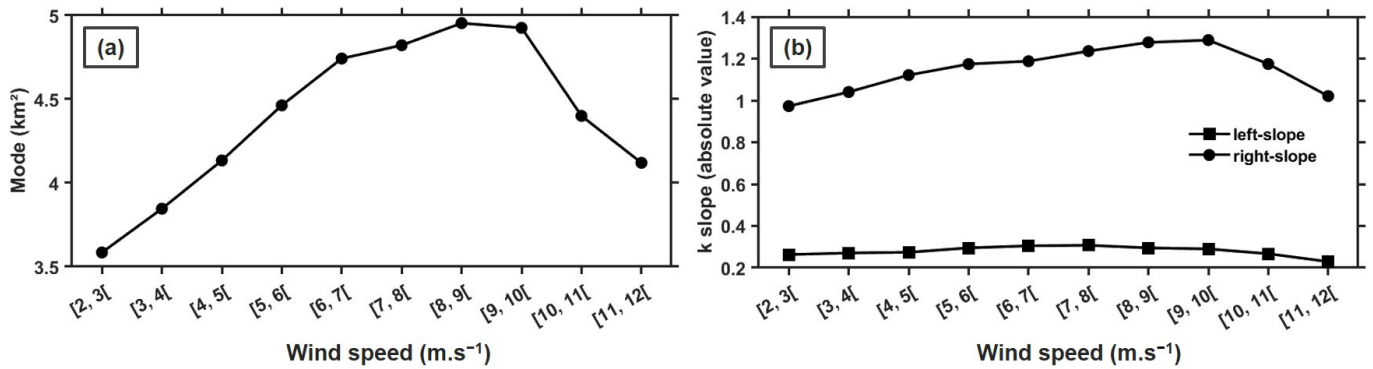


Figure 13. Mode (a) and absolute value (b) of the left-slope (dots) and right-slope (squares) of the surface area distribution for each wind class.

4. Discussion

4.1. Does the Cloud Fraction Bias Our Observations?

The presence of clouds in satellite imagery interferes with sea surface observations. It is conventional to say that cloud edges and shadows generally lead to false detections by index methods [34]. The method used in this paper, based on convolutional neural networks, avoids such difficulties by reducing the number of false detections [39]. Furthermore, the *Sargassum* fraction remains the same for all cloud coverages considered in this study (from 0 to 0.7), as illustrated in Figure 4.

The decrease observed between 2 and 12 m·s⁻¹ wind speed (Section 3.3.1) occurs while the cloud fraction is quasi-constant (between 0.20 and 0.33), illustrating that the *Sargassum* fraction is less influenced by cloud fraction (which ranges from 0.20 to 0.33, Figure 14) than by wind speed. Then, around 13 m·s⁻¹, while the cloud fraction is still 0.35, the *Sargassum* fraction is almost 0. Therefore, the wind effect seems predominant in the decrease in the *Sargassum* fraction.

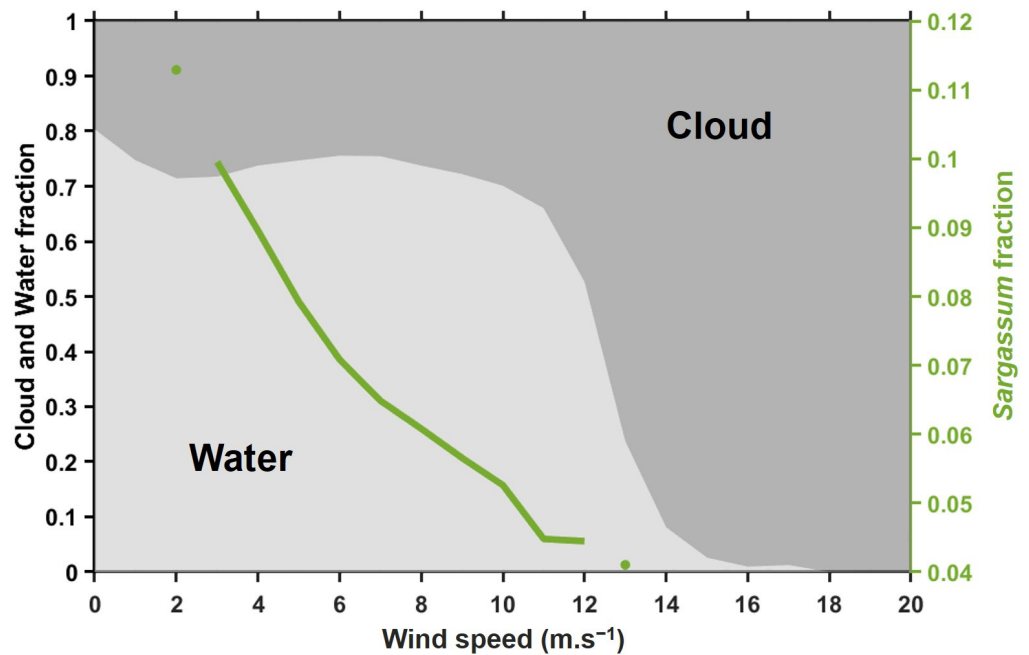


Figure 14. Water, cloud (left y-axis), and *Sargassum* (right y-axis) fraction in each wind speed class over the *Sargassum* period. *Sargassum* fraction from Figure 12; dots represent the *Sargassum* fraction discarded in wind classes due to insufficient data (Figure 5).

The lack of *Sargassum* pixels in the images for wind classes above $12 \text{ m}\cdot\text{s}^{-1}$ (Figure 5) could be associated with the lack or disappearance of *Sargassum* in the images during high wind events or the impossibility of detecting the presence of *Sargassum* by OLCI due to high wind speeds and wavy conditions. Furthermore, below $2 \text{ m}\cdot\text{s}^{-1}$, no data were considered because these wind speeds are mostly associated with the *Sargassum* low season (October to December), which is not part of our sample (Figure 6).

4.2. Disaggregation and Agglomeration of *Sargassum* Aggregations by Wind

Sargassum aggregations result either from the disaggregation of larger aggregations or from the agglomeration of smaller aggregations. On the one hand, the wind favors encounters between isolated *Sargassum* that can agglomerate. On the other hand, the wind induces water and atmospheric movements that can fragment existing *Sargassum* aggregations. The dominant effect depends on the size of aggregations and the wind speed. Large rafts of *Sargassum* are more likely to be observed when the sea is calm [22]. *Sargassum* rafts start to disaggregate with wind speed above $4 \text{ m}\cdot\text{s}^{-1}$, according to Woodcock et al. [26], or $5 \text{ m}\cdot\text{s}^{-1}$ according to Marmorino et al. [28].

Assuming a homogeneous disaggregation or agglomeration, the power law proposed for the area distribution of aggregations (Equation (4)) assumes that the frequency of the number of elements F_{i+1} in area class A_{i+1} (Equation (4)) can be expressed by the frequency of the number of elements F_i in the lower area class A_i . Then, from Equations (3) and (5), we can write

$$F_{i+1} = 2^k F_i \quad (5)$$

The slope k characterizes the disaggregation level (in absolute value) of the aggregation distribution. A distribution with a low level of segmentation is characterized by a large value of the left slope and a low absolute value of the right slope. When the distribution becomes more fragmented, the left slope decreases, while the right slope becomes steeper. At the same time, the mode shifts to the left, and the mean area value decreases.

For lower wind speeds (from 2 to $9 \text{ m}\cdot\text{s}^{-1}$), the mode shifts to the right as wind speed increases (Figure 13), both k -slopes increase, the size distribution tightens, and the number of both the smallest and largest aggregations decreases (Figure 15). This indicates that smaller aggregations in the left-subset agglomerate as the wind speed increases, whereas larger aggregations in the right-subset fragment. The first process populates area classes in the lower modal range, while the second process populates area classes in the upper modal range. This explains the higher occurrence of aggregations in the modal range of the size distribution due to the cumulative effect of agglomeration of smaller aggregations and disaggregation of larger ones.

For stronger wind (above $9 \text{ m}\cdot\text{s}^{-1}$), the mode shifts to the left as wind speed increases (Figure 13), and the left slope decreases, whereas the absolute value of the right slope increases, i.e., the overall distribution is shifted to the left, hence the number of largest aggregations decreases while the number of smaller aggregations increases (Figure 15). This confirms an overall disaggregation of the *Sargassum* aggregations in high wind conditions. Note that Figure 13 seems to indicate that the disaggregation process weakens above $10 \text{ m}\cdot\text{s}^{-1}$ as the absolute value of the k slope decreases. However, the calculation of k for the right subset is not reliable above $10 \text{ m}\cdot\text{s}^{-1}$ because the area classes corresponding to the largest aggregations are empty. The very fact that the largest aggregations disappear proves the disaggregation process; hence, the absolute value of the k slope should keep increasing as the wind speed increases.

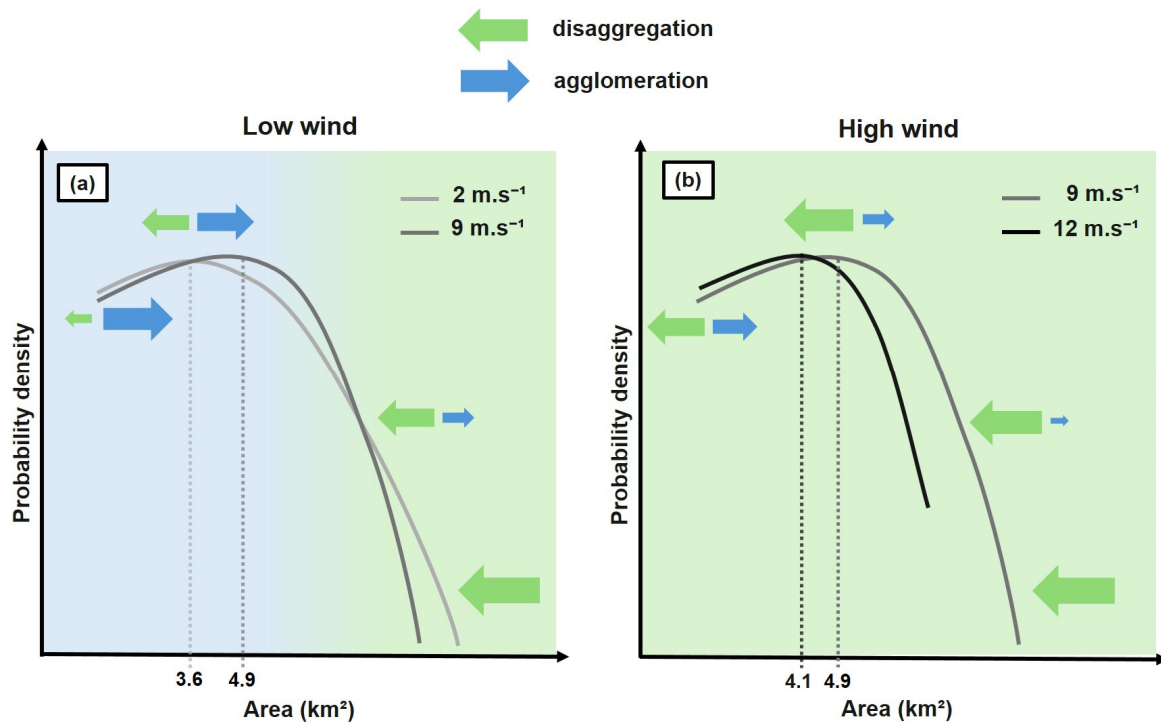


Figure 15. Schematic representation of the evolution of the size distribution with wind, from a lower wind speed (black curve) to a higher wind speed (red curve) for (a) low to moderate wind conditions, from 2 to 9 $\text{m}\cdot\text{s}^{-1}$ and for (b) high wind conditions, from 9 to 12 $\text{m}\cdot\text{s}^{-1}$. The background colour indicates the dominant process: disaggregation (blue) or agglomeration (green).

In conclusion, in low to moderate wind conditions (from 2 to 9 $\text{m}\cdot\text{s}^{-1}$), wind increase favors the agglomeration of smaller *Sargassum* aggregations and the disaggregation of larger aggregations. In high wind conditions (above 9 $\text{m}\cdot\text{s}^{-1}$), wind increase favors the disaggregation of all aggregations.

4.3. Effect of Wind on the Decrease in *Sargassum* Fraction

In low to moderate wind conditions (from 2 to 9 $\text{m}\cdot\text{s}^{-1}$), the decrease in *Sargassum* fraction in satellite imagery as wind speed increases (Section 3.1.1.) can be explained by the agglomeration of small *Sargassum* aggregations inducing a decrease in the observed *Sargassum* surface.

In high wind conditions (above 9 $\text{m}\cdot\text{s}^{-1}$), the decrease in *Sargassum* fraction can be explained by the dispersal and disaggregation processes that may cause a gradual loss of *Sargassum* detection. Firstly, the smallest aggregations may become too small and too dispersed to be detected by OLCI due to their resolution [45]. Secondly, windy conditions induce waves that can submerge aggregations and make them undetectable in satellite imagery [24,26,46]. Finally, high wind conditions may induce *Sargassum* algal mortality, as wind stress can damage the aerocysts that keep *Sargassum* floating on the surface, causing them to sink and die [30].

4.4. Spatial Variability of Disaggregation and Agglomeration of *Sargassum* Aggregations

The rafts move mainly from the east (Atlantic) to the west (Caribbean). In the Lesser Antilles Arc, the funnel effect, in association with the topography and the eddies generated by return currents in the lee of the islands [47], creates biological accumulation zones [48,49] and favors the accumulation of aggregations. Hence, aggregations from the Atlantic offshore (AZ zone) become larger when they arrive in the Lesser Antilles Arc (AAZ and CAZ zones): the mode value increases with fewer smaller aggregations (left slope increase)

and more larger aggregations (right slope increase). The phenomenon is more pronounced on the lee side (West side) of the Lesser Antilles islands (CAZ zone), where the mode value is the highest (6.82 km²), and the right slope is maximal as well (−1.04). This is confirmed by the observations of Ody et al. [24] and Goodwin et al. [27] during their at-sea campaign, where the largest rafts were found around the Caribbean coasts of the Lesser Antilles islands.

Once in the Caribbean offshore part (CZ zone), aggregations fall under similar conditions as the Atlantic offshore part (AZ zone), which are less favorable to agglomeration and where huge aggregations become rare (the absolute right-slope increases). However, aggregations remain larger in the Caribbean Sea than in the Atlantic (mode value of 5.35 km² in CZ against 3.56 km² in AZ; Figure 11a). This can be explained by the higher wind speed found in the Caribbean Sea than in the Atlantic Ocean (2 m·s^{−1} stronger; Figure 6); the aggregations would be more frequent in the high wind classes of the low wind regime (from 2 to 9 m·s^{−1}; Figure 15), i.e., the size of the aggregations would increase towards the modal value.

The coastal zone has a different condition than the other zones, more impacted by disaggregation, consistent with the observations of sea users in Martinique who report that rafts are smaller near coasts.

5. Conclusions

This study analyzed four years of OLCI *Sargassum* imagery in the West Indies, beyond the seasonal and interannual variability described by several authors [2,43]. This study focused on the effect of wind speed on *Sargassum* spatial distribution and segmentation. The analysis emphasized the following findings:

- The *Sargassum* coverage decreases with wind speed and reaches zero when wind speed reaches 13 m·s^{−1}. While agglomeration explains that tendency for lower wind speeds, the decrease in *Sargassum* fraction for higher wind speeds disaggregation indicates either a lesser detectability or a loss of *Sargassum* amount;
- The size distribution of *Sargassum* aggregations results from two opposite processes, mainly driven by wind: agglomeration and disaggregation;
 - In low to moderate wind conditions (from 2 to 9 m·s^{−1}), wind has a dual effect: it agglomerates smaller aggregations and disaggregates larger ones. In these wind regimes, the agglomeration process dominates, increasing the average size of aggregations;
 - In higher wind conditions (above 9 m·s^{−1}), disaggregation outweighs agglomeration, inducing a decrease in the average size of aggregations.

The size distribution varies spatially. On the one hand, it is influenced by the different wind regimes between the Caribbean and the Atlantic. In the Caribbean, winds are stronger in the low–moderate wind range (2 to 9 m·s^{−1}) than in the Atlantic, which increases agglomeration. On the other hand, the topography between the Lesser Antilles Arc, the offshore areas, and the coastal areas also influences the size distribution. In contrast to offshore areas, the islands of the Lesser Antilles Arc are accumulation areas that favor agglomeration. In addition, coastal areas favor disaggregation due to wave and tidal dynamics, which intensify in coastal areas.

This study contributes to a better understanding of the dynamics of disaggregation and agglomeration of *Sargassum* rafts and the response of *Sargassum* spatial distribution to wind. Such knowledge is of interest to improve the modeling of *Sargassum* growth and transport and, ultimately, the prediction of *Sargassum* stranding events. Short-term and long-term predictions are key tools to help populations affected by *Sargassum* inundation,

offering decision-makers and local authorities the possibility to adapt their prevention and mitigation strategies to the influx of *Sargassum* approaching the coast.

Author Contributions: Conceptualization, M.L., Y.A., J.D., L.C. and C.C.; methodology, M.L., L.C., J.D. and C.C.; software, J.D., L.C. and A.S.-G.; formal analysis, M.L., Y.A., J.D., L.C. and C.C.; resources, M.L., J.D. and L.C.; data curation, M.L., J.D. and C.C.; writing—original draft preparation, M.L., Y.A., J.D. and C.C.; writing—review and editing, Y.A., J.D., L.C., P.D.-N., A.C.d.S., P.Z., R.D. and C.C.; supervision, C.C.; funding acquisition, R.D. and P.Z. All authors have read and agreed to the published version of the manuscript.

Funding: This research was funded by the National Research Agency (ANR) in the SargAlert project (grant number: ANR-22-SARG-0001-01), FACEPE (grant number: APQ-0411-1.08/22) and by the Territorial Authority of Martinique (CTM; grant number: MQ0027405).

Data Availability Statement: The OLCI *Sargassum* data set used in this study will be made available through the web portal of the SargAlert Project at <https://sargalert.lis-lab.fr> (accessed on 25 October 2024). In the meantime, they are available on request from the corresponding author.

Acknowledgments: The authors would like to thank Copernicus Open Access Hub for providing Sentinel-3/OLCI data.

Conflicts of Interest: The authors declare no conflicts of interest.

Appendix A

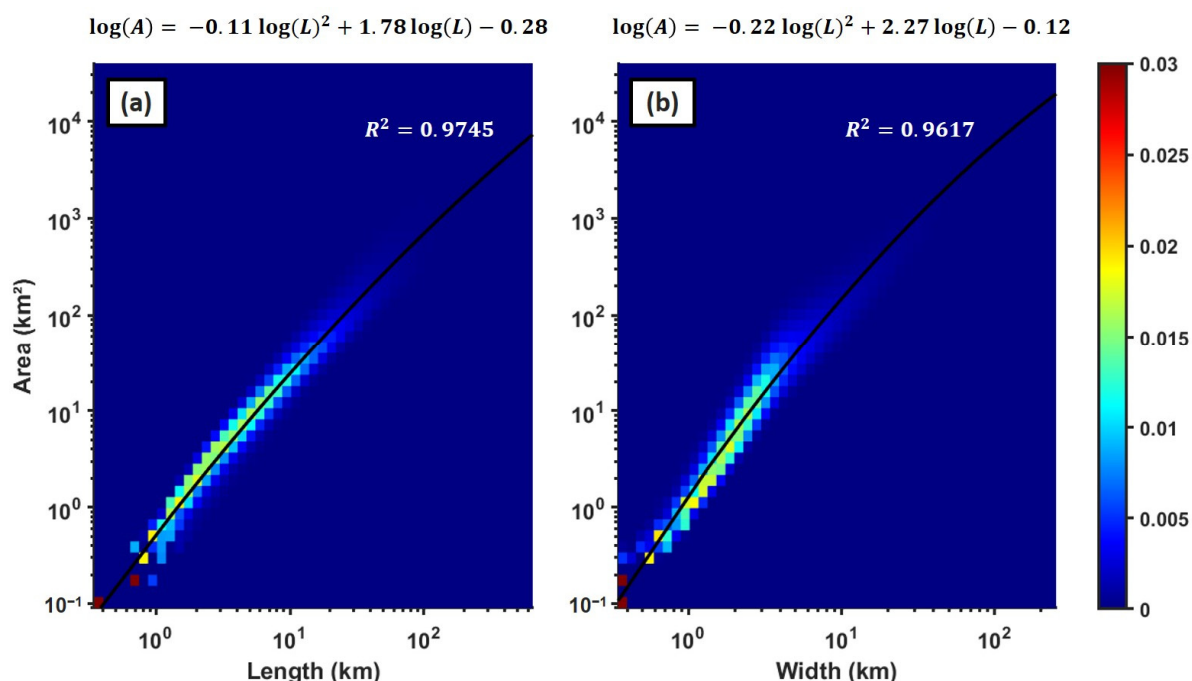


Figure A1. Density plot of the area of *Sargassum* aggregations as a function of their length (a) and width (b), presented by the logarithmic scale axis. The color scale represents the probability density. Area, length, and width are from the entire dataset. The black line represents a second-order polynomial fitting the distribution of the *Sargassum* area as a function of their length (a) and (b) width ($R^2 = 0.97$ and 0.96 , respectively).

References

1. Ardron, J.; Halpin, P.; Roberts, J.; Cleary, J.; Moffitt, R.; Donnelly, B. *Where Is the Sargasso Sea? Sargasso Sea Alliance Science Report Series*; Duke University Marine Geospatial Ecology Lab & Marine Conservation Institute: Beaufort, NC, USA, 2011; 24p.
2. Wang, M.; Hu, C.; Barnes, B.B.; Mitchum, G.; Lapointe, B.; Montoya, J.P. The Great Atlantic *Sargassum* Belt. *Science* **2019**, *365*, 83–87. [[CrossRef](#)] [[PubMed](#)]

3. de Széchy, M.T.M.; Guedes, P.M.; Baeta-Neves, M.H.; Oliveira, E.N. Verification of *Sargassum natans* (Linnaeus) Gaillon (Heterokontophyta: Phaeophyceae) from the Sargasso Sea off the Coast of Brazil, Western Atlantic Ocean. *Check List* **2012**, *8*, 638–641. [[CrossRef](#)]
4. Gower, J.; Young, E.; King, S. Satellite Images Suggest a New *Sargassum* Source Region in 2011. *Remote Sens. Lett.* **2013**, *4*, 764–773. [[CrossRef](#)]
5. Smetacek, V.; Zingone, A. Green and Golden Seaweed Tides on the Rise. *Nature* **2013**, *504*, 84–88. [[CrossRef](#)]
6. Maréchal, J.-P.; Hellio, C.; Hu, C. A Simple, Fast, and Reliable Method to Predict *Sargassum* Washing Ashore in the Lesser Antilles. *Remote Sens. Appl. Soc. Environ.* **2017**, *5*, 54–63. [[CrossRef](#)]
7. Trinanes, J.; Putman, N.F.; Goni, G.; Hu, C.; Wang, M. Monitoring Pelagic *Sargassum* Inundation Potential for Coastal Communities. *J. Oper. Oceanogr.* **2023**, *16*, 48–59. [[CrossRef](#)]
8. Chávez, V.; Uribe-Martínez, A.; Cuevas, E.; Rodríguez-Martínez, R.E.; van Tussenbroek, B.I.; Francisco, V.; Estévez, M.; Celis, L.B.; Monroy-Velázquez, L.V.; Leal-Bautista, R.; et al. Massive Influx of Pelagic *Sargassum* spp. on the Coasts of the Mexican Caribbean 2014–2020: Challenges and Opportunities. *Water* **2020**, *12*, 2908. [[CrossRef](#)]
9. Schling, M.; Guerrero Compeán, R.; Pazos, N.; Bailey, A.; Arkema, K.; Ruckelshaus, M. *The Economic Impact of Sargassum: Evidence from the Mexican Coast*; IDB Working Paper Series; Inter-American Development Bank (IDB): Washington, DC, USA, 2022. [[CrossRef](#)]
10. van Tussenbroek, B.I.; Hernández Arana, H.A.; Rodríguez-Martínez, R.E.; Espinoza-Avalos, J.; Canizales-Flores, H.M.; González-Godoy, C.E.; Barba-Santos, M.G.; Vega-Zepeda, A.; Collado-Vides, L. Severe Impacts of Brown Tides Caused by *Sargassum* spp. on near-Shore Caribbean Seagrass Communities. *Mar. Pollut. Bull.* **2017**, *122*, 272–281. [[CrossRef](#)]
11. Rodríguez-Martínez, R.E.; Medina-Valmaseda, A.E.; Blanchon, P.; Monroy-Velázquez, L.V.; Almazán-Becerril, A.; Delgado-Pech, B.; Vásquez-Yeomans, L.; Francisco, V.; García-Rivas, M.C. Faunal Mortality Associated with Massive Beaching and Decomposition of Pelagic *Sargassum*. *Mar. Pollut. Bull.* **2019**, *146*, 201–205. [[CrossRef](#)]
12. Maurer, A.S.; Stapleton, S.P.; Layman, C.A.; Burford Reiskind, M.O. The Atlantic *Sargassum* Invasion Impedes Beach Access for Nesting Sea Turtles. *Clim. Chang. Ecol.* **2021**, *2*, 100034. [[CrossRef](#)]
13. Maurer, A.S.; Gross, K.; Stapleton, S.P. Beached *Sargassum* Alters Sand Thermal Environments: Implications for Incubating Sea Turtle Eggs. *J. Exp. Mar. Biol. Ecol.* **2022**, *546*, 151650. [[CrossRef](#)]
14. Resiere, D.; Valentino, R.; Nevière, R.; Banydeen, R.; Gueye, P.; Florentin, J.; Cabié, A.; Lebrun, T.; Mégarbane, B.; Guerrier, G.; et al. *Sargassum* Seaweed on Caribbean Islands: An International Public Health Concern. *Lancet* **2018**, *392*, 2691. [[CrossRef](#)] [[PubMed](#)]
15. Resiere, D.; Mehdaoui, H.; Florentin, J.; Gueye, P.; Lebrun, T.; Bateau, A.; Viguier, J.; Valentino, R.; Brouste, Y.; Kallel, H.; et al. *Sargassum* Seaweed Health Menace in the Caribbean: Clinical Characteristics of a Population Exposed to Hydrogen Sulfide during the 2018 Massive Stranding. *Clin. Toxicol.* **2021**, *59*, 215–223. [[CrossRef](#)] [[PubMed](#)]
16. de Lanlay, D.B.; Monthieux, A.; Banydeen, R.; Jean-Laurent, M.; Resiere, D.; Drame, M.; Nevière, R. Risk of Preeclampsia among Women Living in Coastal Areas Impacted by *Sargassum* Strandings on the French Caribbean Island of Martinique. *Environ. Toxicol. Pharmacol.* **2022**, *94*, 103894. [[CrossRef](#)]
17. Liranzo-Gómez, R.E.; Gómez, A.M.; Gómez, B.; González-Hernández, Y.; Jauregui-Haza, U.J. Characterization of *Sargassum* Accumulated on Dominican Beaches in 2021: Analysis of Heavy, Alkaline and Alkaline-Earth Metals, Proteins and Fats. *Mar. Pollut. Bull.* **2023**, *193*, 115120. [[CrossRef](#)]
18. Silva, T.M.; Waked, D.; Bastos, A.C.; Gomes, G.L.; Veras Closs, J.G.; Tonin, F.G.; Rossignolo, J.A.; Do Valle Marques, K.; Veras, M.M. A Custom, Low-Cost, Continuous Flow Chamber Built for Experimental *Sargassum* Seaweed Decomposition and Exposure of Small Rodents to Generated Gaseous Products. *Heliyon* **2023**, *9*, e18787. [[CrossRef](#)]
19. Schell, J.M.; Goodwin, D.S.; Siuda, A.N.S. Recent *Sargassum* Inundation Events in the Caribbean: Shipboard Observations Reveal Dominance of a Previously Rare Form. *Oceanography* **2015**, *28*, 8–11. [[CrossRef](#)]
20. Amaral-Zettler, L.A.; Dragone, N.B.; Schell, J.; Slikas, B.; Murphy, L.G.; Morrall, C.E.; Zettler, E.R. Comparative Mitochondrial and Chloroplast Genomics of a Genetically Distinct Form of *Sargassum* Contributing to Recent “Golden Tides” in the Western Atlantic. *Ecol. Evol.* **2017**, *7*, 516–525. [[CrossRef](#)]
21. Dibner, S.; Martin, L.; Thibaut, T.; Aurelle, D.; Blanfuné, A.; Whittaker, K.; Cooney, L.; Schell, J.M.; Goodwin, D.S.; Siuda, A.N.S. Consistent Genetic Divergence Observed among Pelagic *Sargassum* Morphotypes in the Western North Atlantic. *Mar. Ecol.* **2022**, *43*, e12691. [[CrossRef](#)]
22. Parr, A. Quantitative Observations on the Pelagic *Sargassum* Vegetation of the Western North Atlantic. With Preliminary Discussion of Morphology and Relationships. *Bull. Bingham Oceanogr. Collect.* **1939**, *6*, 7.
23. Butler, J.N.; Stoner, A.W. Pelagic *Sargassum*: Has Its Biomass Changed in the Last 50 Years? *Deep Sea Res. Part A Oceanogr. Res. Pap.* **1984**, *31*, 1259–1264. [[CrossRef](#)]
24. Ody, A.; Thibaut, T.; Berline, L.; Changeux, T.; André, J.-M.; Chevalier, C.; Blanfuné, A.; Blanchot, J.; Ruitton, S.; Stiger-Pouvreau, V.; et al. From In Situ to Satellite Observations of Pelagic *Sargassum* Distribution and Aggregation in the Tropical North Atlantic Ocean. *PLoS ONE* **2019**, *14*, e0222584. [[CrossRef](#)]

25. Woodcock, A. Subsurface Pelagic *Sargassum*. *J. Mar. Res.* **1950**, *9*. Available online: https://elischolar.library.yale.edu/journal_of_marine_research/722 (accessed on 25 October 2024).
26. Woodcock, A.H. Winds Subsurface Pelagic *Sargassum* and Langmuir Circulations. *J. Exp. Mar. Biol. Ecol.* **1993**, *170*, 117–125. [[CrossRef](#)]
27. Goodwin, D.S.; Siuda, A.N.S.; Schell, J.M. In Situ Observation of Holopelagic *Sargassum* Distribution and Aggregation State across the Entire North Atlantic from 2011 to 2020. *PeerJ* **2022**, *10*, e14079. [[CrossRef](#)] [[PubMed](#)]
28. Marmorino, G.O.; Miller, W.D.; Smith, G.B.; Bowles, J.H. Airborne Imagery of a Disintegrating *Sargassum* Drift Line. *Deep Sea Res. Part I Oceanogr. Res. Pap.* **2011**, *58*, 316–321. [[CrossRef](#)]
29. Langmuir, I. Surface Motion of Water Induced by Wind. *Science* **1938**, *87*, 119–123. [[CrossRef](#)]
30. Sosa-Gutierrez, R.; Jouanno, J.; Berline, L.; Descloitres, J.; Chevalier, C. Impact of Tropical Cyclones on Pelagic *Sargassum*. *Geophys. Res. Lett.* **2022**, *49*, e2021GL097484. [[CrossRef](#)]
31. Sun, Y.; Wang, M.; Liu, M.; Li, Z.B.; Chen, Z.; Huang, B. Continuous *Sargassum* Monitoring across the Caribbean Sea and Central Atlantic Using Multi-Sensor Satellite Observations. *Remote Sens. Environ.* **2024**, *309*, 114223. [[CrossRef](#)]
32. Berline, L.; Ody, A.; Jouanno, J.; Chevalier, C.; André, J.-M.; Thibaut, T.; Ménard, F. Hindcasting the 2017 Dispersal of *Sargassum* Algae in the Tropical North Atlantic. *Mar. Pollut. Bull.* **2020**, *158*, 111431. [[CrossRef](#)]
33. Bernard, D.; Biabiany, E.; Cécé, R.; Chery, R.; Sekkat, N. Clustering Analysis of the *Sargassum* Transport Process: Application to Beaching Prediction in the Lesser Antilles. *Ocean Sci.* **2022**, *18*, 915–935. [[CrossRef](#)]
34. Wang, M.; Hu, C. Mapping and Quantifying *Sargassum* Distribution and Coverage in the Central West Atlantic Using MODIS Observations. *Remote Sens. Environ.* **2016**, *183*, 350–367. [[CrossRef](#)]
35. Putman, N.F.; Goni, G.J.; Gramer, L.J.; Hu, C.; Johns, E.M.; Trinanés, J.; Wang, M. Simulating Transport Pathways of Pelagic *Sargassum* from the Equatorial Atlantic into the Caribbean Sea. *Prog. Oceanogr.* **2018**, *165*, 205–214. [[CrossRef](#)]
36. Franks, J.S.; Johnson, D.R.; Ko, D.S.; Sanchez-Rubio, G.; Hendon, J.R.; Lay, M. Unprecedented Influx of Pelagic *Sargassum* along Caribbean Island Coastlines during Summer 2011. In *Proceedings of the 64th Gulf and Caribbean Fisheries Institute; Gulf and Caribbean Fisheries Institute: Puerto Morelos, Mexico, 2012*; pp. 6–8.
37. Franks, J.S.; Johnson, D.R.; Ko, D.S. Pelagic *Sargassum* in the Tropical North Atlantic. *GCR* **2016**, *27*, SC6–SC11. [[CrossRef](#)]
38. Andrade-Canto, F.; Beron-Vera, F.J.; Goni, G.J.; Karrasch, D.; Olascoaga, M.J.; Triñanes, J. Carriers of *Sargassum* and Mechanism for Coastal Inundation in the Caribbean Sea. *Phys. Fluids* **2022**, *34*, 016602. [[CrossRef](#)]
39. Laval, M.; Belmouhcine, A.; Courtrai, L.; Descloitres, J.; Salazar-Garibay, A.; Schamberger, L.; Minghelli, A.; Thibaut, T.; Dorville, R.; Mazoyer, C.; et al. Detection of *Sargassum* from Sentinel Satellite Sensors Using Deep Learning Approach. *Remote Sens.* **2023**, *15*, 1104. [[CrossRef](#)]
40. Hersbach, H.; Bell, B.; Berrisford, P.; Biavati, G.; Horányi, A.; Muñoz Sabater, J.; Nicolas, J.; Peubey, C.; Radu, R.; Rozum, I.; et al. ERA5 Hourly Data on Single Levels from 1940 to Present. 2018. Available online: <https://cds.climate.copernicus.eu/datasets/reanalysis-era5-single-levels?tab=overview> (accessed on 25 October 2024).
41. Nordkvist, K.; Loisel, H.; Gaurier, L.D. Cloud Masking of SeaWiFS Images over Coastal Waters Using Spectral Variability. *Opt. Express OE* **2009**, *17*, 12246–12258. [[CrossRef](#)]
42. Schamberger, L.; Minghelli, A.; Chami, M.; Steinmetz, F. Improvement of Atmospheric Correction of Satellite Sentinel-3/OLCI Data for Oceanic Waters in Presence of *Sargassum*. *Remote Sens.* **2022**, *14*, 386. [[CrossRef](#)]
43. Brooks, M.; Coles, V.; Hood, R.; Gower, J. Factors Controlling the Seasonal Distribution of Pelagic *Sargassum*. *Mar. Ecol. Prog. Ser.* **2018**, *599*, 1–18. [[CrossRef](#)]
44. Jouanno, J.; Morvan, G.; Berline, L.; Benshila, R.; Aumont, O.; Sheinbaum, J.; Ménard, F. Skillful Seasonal Forecast of *Sargassum* Proliferation in the Tropical Atlantic. *Geophys. Res. Lett.* **2023**, *50*, e2023GL105545. [[CrossRef](#)]
45. Putman, N.F.; Hu, C. Sinking *Sargassum*. *Geophys. Res. Lett.* **2022**, *49*, e2022GL100189. [[CrossRef](#)]
46. Schamberger, L.; Minghelli, A.; Chami, M. Quantification of Underwater *Sargassum* Aggregations Based on a Semi-Analytical Approach Applied to Sentinel-3/OLCI (Copernicus) Data in the Tropical Atlantic Ocean. *Remote Sens.* **2022**, *14*, 5230. [[CrossRef](#)]
47. De Falco, C.; Desbiolles, F.; Bracco, A.; Pasquero, C. Island Mass Effect: A Review of Oceanic Physical Processes. *Front. Mar. Sci.* **2022**, *9*. [[CrossRef](#)]
48. Boehlert, G.W.; Watson, W.; Sun, L.C. Horizontal and Vertical Distributions of Larval Fishes around an Isolated Oceanic Island in the Tropical Pacific. *Deep Sea Res. Part A Oceanogr. Res. Pap.* **1992**, *39*, 439–466. [[CrossRef](#)]
49. Wilson, B.; Hayek, L.-A.C. Islands, Currents, Eddies, Fronts... and Benthic Foraminifera: Controls on Neritic Distributions off Trinidad. *Micropaleontology* **2017**, *63*, 15–26. [[CrossRef](#)]

Disclaimer/Publisher’s Note: The statements, opinions and data contained in all publications are solely those of the individual author(s) and contributor(s) and not of MDPI and/or the editor(s). MDPI and/or the editor(s) disclaim responsibility for any injury to people or property resulting from any ideas, methods, instructions or products referred to in the content.